Extreme Mechanics Letters 42 (2021) 101134

Contents lists available at ScienceDirect

Extreme Mechanics Letters

journal homepage: www.elsevier.com/locate/eml

Antagonistic cone dielectric elastomer actuator: Analysis, experiment and application

Yaguang Guo [a], Liwu Liu [a,*], Yanju Liu [a], Jinsong Leng [b,*]

[a] Department of Astronautical Science and Mechanics, Harbin Institute of Technology (HIT), P.O. Box 301, No. 92 West Dazhi Street, Harbin 150001, People's Republic of China

[b] Center for Composite Materials and Structures, Science Park of Harbin Institute of Technology (HIT), P.O. Box 3011, No. 2 YiKuang Street, Harbin 150080, People's Republic of China

ARTICLE INFO

Article history:
Received 9 August 2020
Received in revised form 1 December 2020
Accepted 2 December 2020
Available online 8 December 2020

Keywords:
Dielectric elastomer
Antagonistic cone dielectric elastomer actuator
Pump
Artificial heart

ABSTRACT

As a typical electroactive polymer, dielectric elastomer can be used in the research of actuators, sensors, and soft robots. The cone actuator, as a representative dielectric elastomer actuator, suffers from the limitation of deformation range. In this work, an antagonistic cone dielectric elastomer actuator with large deformation range is exhibited. A theoretical model is derived to design geometric parameters and explain the deformation mechanism of the antagonistic cone dielectric elastomer actuator. Comparison between theoretical and experimental results shows that the theoretical model is suitable for the prediction of the performance of the actuator. Inspired by the human heart, the pump is developed by the actuator, and its performance is systematically investigated through experiments. It is hoped that this work can play a guiding role in the development and application of the antagonistic cone dielectric elastomer actuator.

1. Introduction

Dielectric elastomer is a typical electroactive polymer that can deform under the stimulate of an external electric field. Due to its fast response speed, light weight, and large strain, dielectric elastomer has attracted the attention of many researchers and was used in various applications such as actuators [1–4], energy harvesters [5,6], sensors [7,8], soft robots [9–12], etc. Generally, dielectric elastomer actuator is a sandwiched structure composed of a membrane and compliant electrodes on both surfaces. Dielectric elastomer membrane would expand its area and reduce its thickness due to the Maxwell stress generated by the external electric field.

The cone actuator, which can produce out-of-plane deformation, is a representative dielectric elastomer actuator. Due to its simple structure and easy manufacturing, the cone actuator has been used in the research of pump [13] and cuttlefish robot [14]. It can also be used as micropositioning stage due to its rapid response [15]. To improve its performance, linear bias spring (LBS) and negative-rate bias spring (NBS) system [16] or a diamond four-bar mechanism [17] were used as bias systems to increase the stroke, and stacked dielectric elastomer membranes were used to increase the blocked force [18]. The negative-rate bias spring (NBS) system also allows the actuator to generate bistable phenomena [19,20]. The compliant electrodes were divided into multiple parts so that the cone actuator can generate multiple degrees of freedom. Inspired by biology, the multi-legged walking robot was actuated by the cone actuator with multi-degree-of-freedom [21,22]. Some theoretical models have also been proposed for the interpretation of experimental phenomena and the actuator design [23–26]. When the applied voltage is large, wrinkles appear first in the inner boundary of the cone actuator [25,26]. The relationship between actuator geometry parameters and performance has been theoretically studied [24]. The nonlinear performance has also been described by a dynamic model [27].

In this work, we present an antagonistic cone dielectric elastomer actuator (ACDEA) and focus on the analysis, design, and application of the actuator. Different from the actuator with multi-degree-of-freedom [9], only displacement in the axial direction is considered. For this kind of actuator, a theoretical model was derived to explain nonlinear electromechanical behavior and design geometric parameters. The performance of the actuator was characterized by experiments. Based on working principle of the human heart, a pump that can generate a larger average flow rate at low frequency, avoiding vibration at resonance frequency was developed by the ACDEA. This work organized as follows: the theoretical model and numerical results of the ACDEA are given in Section 2. Section 3 describes the fabrication process and experiment of the ACDEA and the pump, followed by the

* Corresponding authors.
E-mail addresses: liulw@hit.edu.cn (L. Liu), lengjs@hit.edu.cn (J. Leng).

https://doi.org/10.1016/j.eml.2020.101134
2352-4316/

results and discussion of the experiment in Section 4. Finally, the conclusion is given in Section 5.

2. Analytic model of ACDEA

Fig. 1(a) shows the schematic diagram of the antagonistic cone dielectric elastomer actuator. Two rigid frames are supported by four support rods and dielectric elastomer membranes with complaint electrodes are joined together from the center by two cylindrical blocks. Viewed from the side, it looks like two cone actuators are connected together.

2.1. Equilibrium equation

As shown in Fig. 1(b) and (c), the thickness of the dielectric elastomer membrane is H in the initial state. Then the membrane is equi-biaxially pre-stretched λ_p and attached to a rigid frame with a inner radius b. Two cylindrical blocks with radius a in the middle are used to connect the two membranes when the two rigid frames are fixed with a height of h. Considering the axisymmetric deformation of the ACDEA, a material particle R_i moves to a place with coordinates $r_i(R_i)$ and $z_i(R_i)$, where $i = 1, 2$ means the upper part and lower part of the actuator. Then the longitudinal stretch is considered by examining two nearby particles R_i and $R_i + dR_i$. In the reference state, the geometric relationship are $dr_i = \cos\theta_i dl_i$ and $dz_i = \sin\theta_i dl_i$, where dl_i is the distance between two points, and θ_i is the slope at the point R_i. The stretch along the longitude and latitude direction are defined as

$$\lambda_{i1} = dl_i/dR_i \tag{1}$$

$$\lambda_{i2} = r_i/R_i \tag{2}$$

The force is balanced along the z and r directions

$$2\pi HR_i s_{i1}\sin\theta_i = F_i \tag{3}$$

$$\frac{d\left(R_i s_{i1}\cos\theta_i\right)}{dR_i} = s_{i2} \tag{4}$$

where F_i are the bonding force between two membrane, and s_{i1} and s_{i2} are the nominal stress along with the longitude and latitude direction, respectively. The coordination equation is

$$F_1 = F_2 \tag{5}$$

Combining Eqs. (1), (3) and (4), we obtain

$$\frac{dr_i}{dR_i} = \lambda_{i1}\cos\theta_i \tag{6}$$

$$\frac{d\theta_i}{dR_i} = -\frac{s_{i2}}{s_{i1}R_i}\sin\theta_i \tag{7}$$

Consider the nominal electric field $E_i^{\sim} = \Phi_i/H$, where Φ is the external voltage applied on the dielectric elastomer membrane, and combined with Eqs. (2), (4) is rewritten as

$$\left[1-\left(\frac{\Phi_i}{H\sqrt{\mu/\varepsilon}}\frac{r_i}{R_i}\right)^2\right]\lambda_{i1}^4 - \frac{F_i}{2\pi aH\mu}\frac{1}{R_i\sin\theta_i}\lambda_{i1}^3 - \left(\frac{R_i}{r_i}\right)^2 = 0 \tag{8}$$

According to the geometric relationship

$$dz_i = -\tan\theta_i dr_i \tag{9}$$

2.2. Material model

Various constitutive models can be used to describe the nonlinear behavior of soft elastomers [28–30]. Here, we use the Gent model to express the strain energy of dielectric elastomer materials taking into account its strain stiffening effect. For an ideal dielectric elastomer, the relationship between the true electric displacement D and electric field E is $D = E\varepsilon$, where ε is the dielectric constant of the material. The free energy density function can be written as

$$W = -\frac{\mu J_{\lim}}{2}\log\left(1-\frac{\lambda_1^2+\lambda_2^2+\lambda_3^2-3}{J_{\lim}}\right) + \frac{1}{2}\varepsilon E^2 \tag{10}$$

where μ is the shear modulus of the elastomer, and $J_{\lim}$ is a material constant reflecting the stretching limit. Consider the material is incompressible, $\lambda_3 = 1/(\lambda_1\lambda_2)$, $E^{\sim} = \Phi/H = \Phi\lambda_1\lambda_2/H$, $E = D/\varepsilon = D^{\sim}/(\varepsilon\lambda_1\lambda_2)$, where $D^{\sim}$ is the nominal electrical displacement, Eq. (10) is rewritten as

$$W\left(\lambda_1,\lambda_2,\widetilde{D}\right) = -\frac{\mu J_{\lim}}{2}\log\left(1-\frac{\lambda_1^2+\lambda_2^2+\lambda_1^{-2}\lambda_2^{-2}-3}{J_{\lim}}\right) + \frac{D^{\sim 2}}{2\varepsilon}\lambda_1^{-2}\lambda_2^{-2} \tag{11}$$

The nominal stresses along the longitude and latitude direction can be obtained as

$$s_1 = \frac{\partial W\left(\lambda_1,\lambda_2,D^{\sim}\right)}{\partial\lambda_1} \tag{12}$$

$$s_2 = \frac{\partial W\left(\lambda_1,\lambda_2,D^{\sim}\right)}{\partial\lambda_2} \tag{13}$$

The true stress relates to the nominal stress as $\sigma_1 = \lambda_1 s_1$ and $\sigma_2 = \lambda_2 s_2$.

2.3. Numerical results

In the computation, we use the following dimensionless quantities: r-coordinate r_i/a, z-coordinate z_i/a, force $F_i/(2\pi aH\mu)$, voltage $\Phi_i/\left(H\sqrt{\mu/\varepsilon}\right)$, and typical material parameters of VHB4910 material: $H = 1$ mm, $\mu = 40$ kPa, $\varepsilon = 3.98\times10^{-11}$ Fm^{-1}, $J_{\lim} = 120$ [31,32]. The boundary conditions are determined according to the geometric parameters of the ACDEA in Section 3. According to Eqs. (11)–(13), s_{i1} and s_{i2} are obtained by partial derivative, $i = 1, 2$, and then substituted into Eqs. (6)–(9). By assuming the initial value $F_i/(2\pi aH\mu)$, the differential Equations (6), (7) and the algebraic Equation (8) can be solved using the shooting method. Once $r_i(R_i)$ and $\theta_i(R_i)$ are solved, the function $z_i(R_i)$ is determined by integrating Equation (9), subject to the initial condition $\sum z_i(a) = h$.

Theoretical results of the ACDEA with a height of $h = 30$ mm are given here (the results of $h = 25$ mm can be obtained from the supporting information). Fig. 2 plot the deformed shapes of the cross section of the ACDEA. The red and black curves represent the voltage and no voltage applied to the membrane, respectively, and the straight blue lines represent the cylindrical block. When the membrane on one side of the ACDEA is subjected to a voltage, the area of the membrane expands, and the cylindrical blocks shift to the other side. The deformation is reversed when the membrane on the other side is subjected to a voltage. As the voltage increases, the displacement of the cylindrical blocks gradually increases.

Fig. 3 depicts the stretch distribution in the membrane with the voltage applied. In Fig. 3(a), the stretch gradually increases with the voltage increases. When the voltage is fixed, the stretch in the longitude direction gradually decreases from the inside to the outside. Due to constraints on the inner and outer boundaries, the stretch in the latitude direction is constant at the inner and outer ends and reaches a peak in the middle, as shown in Fig. 3(b).

The distribution of true stress is shown in Fig. 4. It can be seen from Fig. 4(a) that the stress σ_1/μ in the longitude direction gradually decreases from the inside to the outside and is always tensile. As the voltage increases, the stress σ_2/μ along the latitude

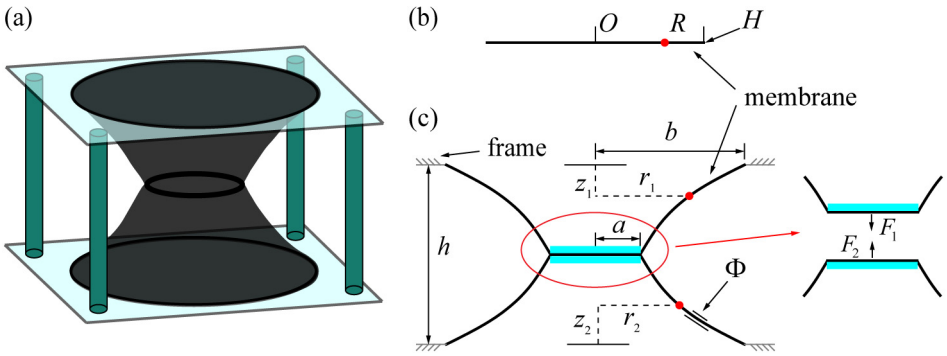

Fig. 1. (a) Schematic illustration of the antagonistic cone dielectric elastomer actuator. (b) The membrane is in the initial state. (c) The cross section of the antagonistic cone dielectric elastomer actuator in the reference state.

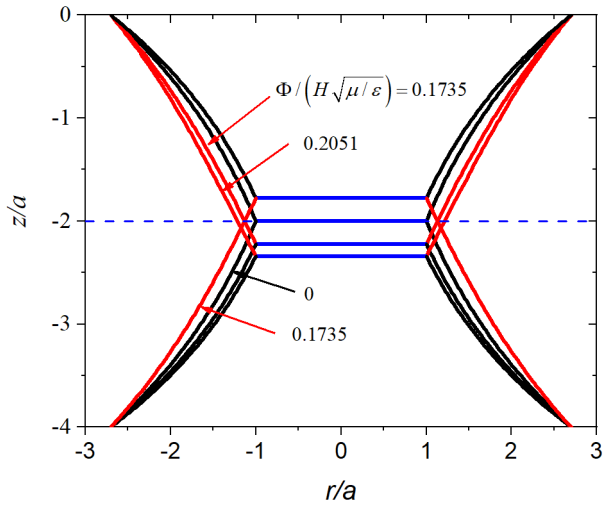

Fig. 2. Deformed shapes of the cross section of the antagonistic cone dielectric elastomer actuator at different voltages. . (For interpretation of the references to color in this figure legend, the reader is referred to the web version of this article.)

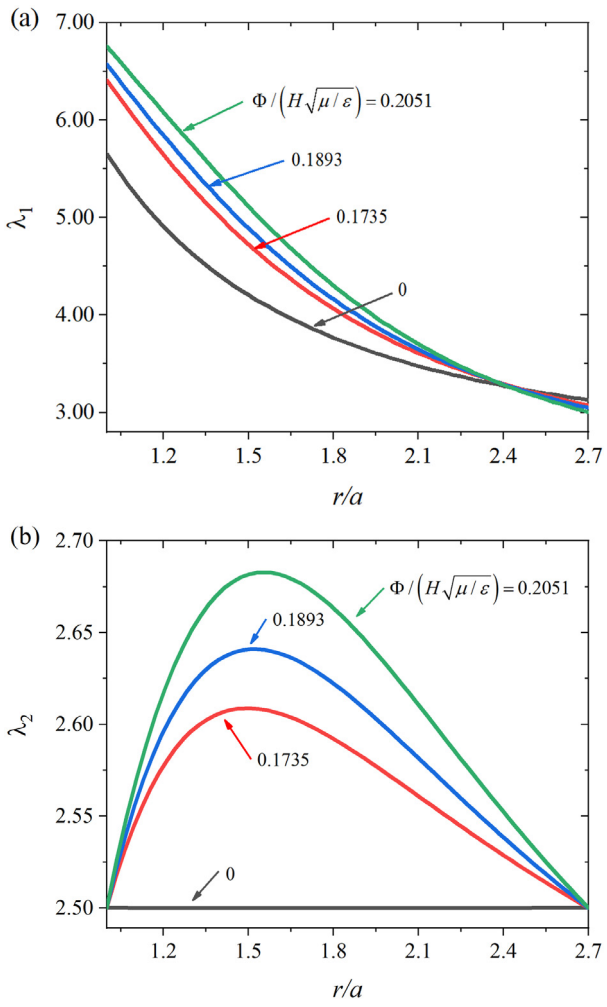

Fig. 3. The distribution of (a) longitudinal stretch and (b) latitudinal stretch.

direction gradually decreases, and when the voltage is about 0.2051, the stress on the inside starts to be less than zero, as shown in Fig. 4b. Assuming that the membrane cannot withstand compressive stress, wrinkles will occur. We also noticed that the latitudinal stress distribution from inside to outside is very uneven. As the voltage increases, the stress near the inside changes greatly. Under the same voltage, the stress distribution from inside to outside changes from gradually decreasing to increasing, and the stress near the outside has almost no change. This uneven stress distribution from inside to outside indicates that the membrane in the outer area is not effectively used.

3. Fabrication and characterization

3.1. Fabrication process

The antagonistic cone dielectric elastomer actuator consists of dielectric elastomer membrane (VHB 4910, 3M Company), polymethyl methacrylate (PMMA) frame, and support rods, etc. As illustrated in Fig. 5(a), two VHB 4910 sheets were pre-stretched biaxially by 2.5×2.5. Carbon grease (MG Chemicals) as the compliant electrodes were symmetrically coated on the surface of dielectric elastomer membrane by using soft brushes and masks. As analyzed in Section 2, wrinkles will be generated first near the interior and then electric field breakdown easily occurs here. To prevent premature electric field breakdown and better use of the outer region of the membrane, the inner diameter of the ring-shaped compliant electrodes is set larger than the outer diameter of the cylindrical block. Two dielectric elastomer membranes with ring-shaped compliant electrodes were concentrically bonded together through the adhesiveness of the material itself. A PMMA frame with an inner diameter of 40 mm was attached to the double-layer dielectric elastomer membrane. When assembling the actuator, four support rods were used to support the PMMA frames while two PMMA cylindrical blocks with a diameter of

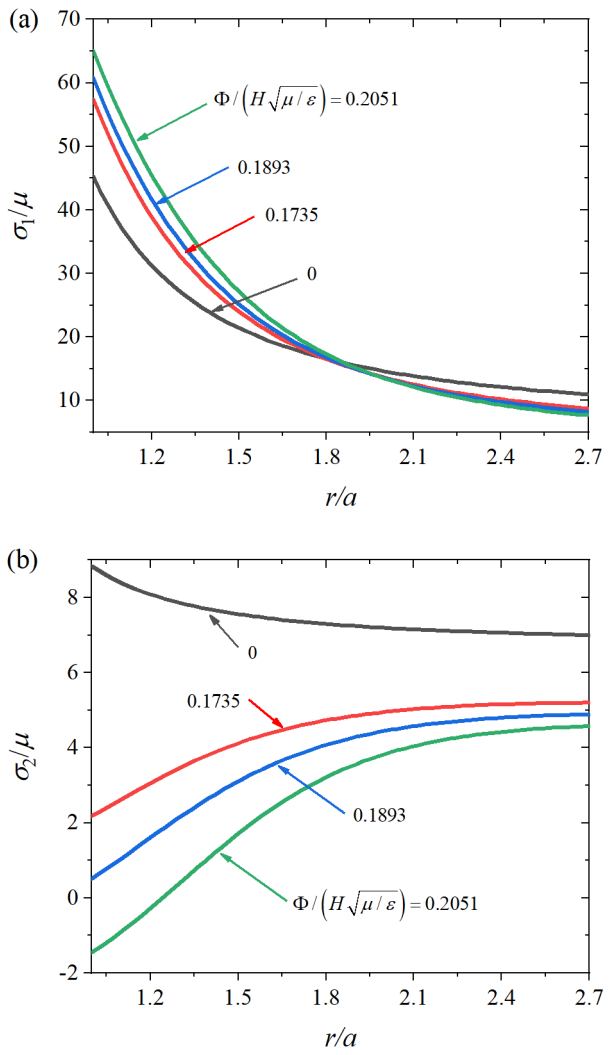

Fig. 4. The distributions of (a) longitudinal true stress and (b) latitudinal true stress.

15 mm were used to join the double-layer dielectric elastomer membrane together, seen in Fig. 5(b).

Inspired by the human heart, a pump was developed by the actuator. Fig. 5(d) shows the composition of the pump shell with check valves. The pump shell was made of a PMMA plate with two holes. The two holes were covered by polydimethylsiloxane (PDMS, Dow Corning, Sylgard 184) film on different sides of the pump shell. Then, two check valve bodies with soft water pipes were connected to the two holes on the same side of the pump shell, respectively. Finally, two pump shells were assembled on both side of the ACDEA to form the pump chamber and ring-shaped PDMS film was used as a seal between the pump shell and the ACDEA, seen in Fig. 5(e). The photograph of the ACDEA and pump were shown in Fig. 5(c) and (f), respectively.

3.2. Working principle

When the one side dielectric elastomer membrane is subjected to a voltage, it expands and tension within them is reduced, the balance of extension forces between two antagonistic cone actuator disappears and the cylindrical block tends to move toward the unactuated side due to the higher tension. It will stop at a new equilibrium point. If the voltage is applied on the other side membrane, it will reach equilibrium at the opposite position.

Fig. 6(a) and (c) briefly describe the process of blood pump. When the ventricles dilate, blood flows into the ventricles, and when the ventricles contract, the blood is expelled from the ventricles. It is slightly different from the simultaneous systole or diastole of the left and right ventricles of the heart to pump blood, as the volume of the pump chamber on the actuated side becomes larger, the outlet check valve closes and the inlet check valve opens, suctioning water into the chamber. The other side of the pump is the opposite, pumping water out of the chamber, as shown in Fig. 6(b) and (d). By applying periodic electrical signals to each side 180° out-of-phase, the antagonistic cone dielectric elastomer pump (ACDEP) can continue pumping water outward.

3.3. Experimental setup

The controlling and measuring system are illustrated in Fig. 7. We use the Arduino UNO to control the two relays to achieve high-voltage which supplied by the high-voltage amplifiers (EMCO Q80-5) on-off. A laser displacement sensor (Panasonic HG-C1050) was used to measure the displacement and a load cell was used to measure the blocked force of the ACDEA. The ACDEP performance was determined using a water reservoir.

First, the quasi-static displacement and blocked force were measured while the ACDEA was subjected to a stepping voltage from 1 kV to 5.5 kV in 0.5 kV steps, each voltage lasting 20 s to ensure the ACDEA was in equilibrium. Then, we fixed voltage to test the dynamic performance of the ACDEA. The displacement was measured at frequencies from 0.5 Hz to 4 Hz. In every measurement, we record at least 10 periods so that their averages could be determined. Finally, the flow rate and pressure of the ACDEP were determined using the same voltage load case as used in the dynamic performance testing. Every experimental condition was repeated 3 times to obtain the average value.

4. Experiment results and discussion

4.1. ACDEA performance

When assembling ACDEA, we can adjust the length of the support rods to change the pre-stretch of the dielectric elastomer membrane. Two types of ACDEA with $h = 25$ mm (H25) and $h = 30$ mm (H30) were made.

Fig. 8(a) depicts the cross section of the ACDEA in the reference state. The green dashed line represents the theoretical result which is in good agreement with the experimental result. Fig. 8(b) shows the displacement–voltage curves of the ACDEA. In the experiment of H30, when the voltage exceeded 6 kV, we observed that wrinkles first appeared in the inner boundary of ring-shaped compliant electrodes, and further increase the voltage slightly, electric field breakdown will occur. As shown in the theoretical analysis results in Section 2, when the voltage exceeds 0.2051 (corresponding to the voltage of 6.5 kV in the experiment), the stress along the latitude direction on the inside starts to be less than zero, which means that wrinkles are generated. It is also consistent with Mao's [26] experimental and theoretical analysis results. To prevent electric field breakdown, we limit the voltage to 5.5 kV.

For convenience, here we use d_L and d_R to represent the displacement when the voltage is applied to the left and right parts of the ACDEA, respectively. As the voltage increases, the displacement gradually increases. When the voltage is higher than 3 kV, the displacement starts to increase rapidly. The cause of this phenomenon may be the occurrence of electromechanical instability or snap-through instability. Comparing the curves of different h, the displacement of H30 is significantly larger than that of H25. The larger pre-stretching can remarkably improve the

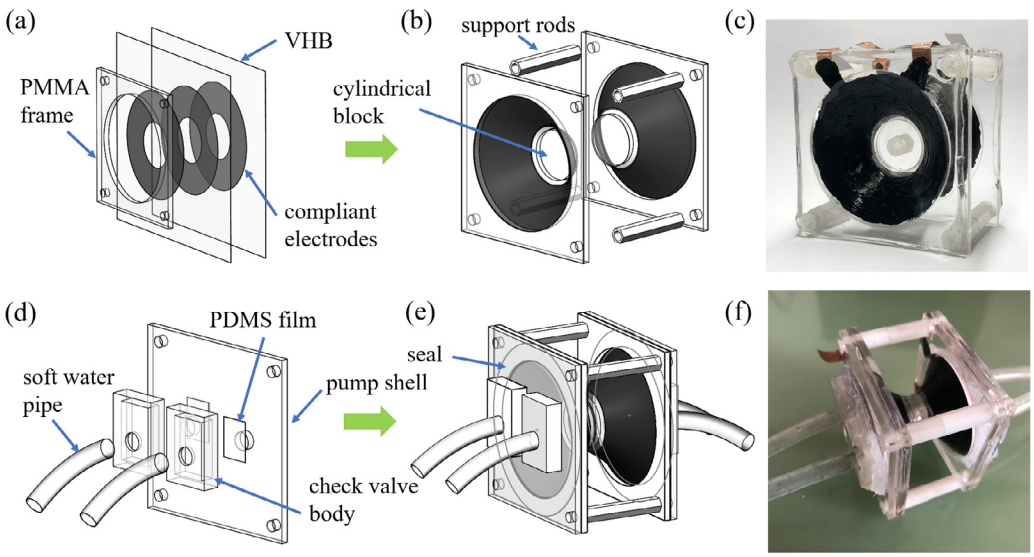

Fig. 5. Schematic description of the fabrication process. (a) Pre-stretched dielectric elastomer membranes with compliant electrodes are attached to the PMMA frame. (b) The frames with dielectric elastomer membrane are assembled into the antagonistic cone dielectric elastomer actuator. (c) Photograph of the antagonistic cone dielectric elastomer actuator. (d) Assembly process of the pump shell with check valves. (d) Schematic diagram and (e) photograph of the pump.

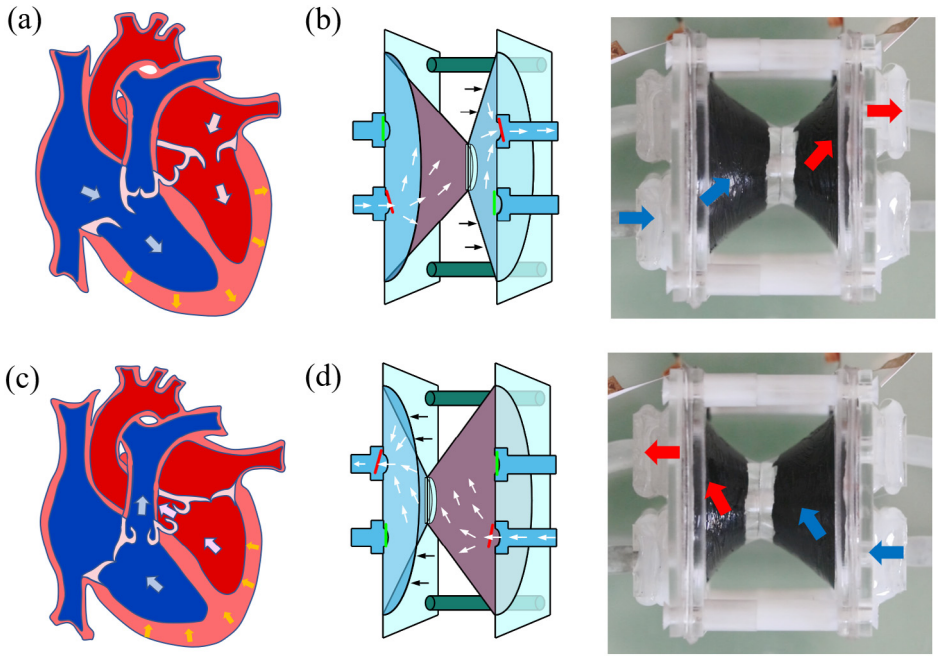

Fig. 6. The schematic diagrams of the working principle of the human heart when (a) blood flowing into the ventricle and (c) being ejected from the ventricle. The working principle of the pump when voltage is applied to the (b) left or (d) right membrane of the pump.

performance of the ACDEA, which is consistent with the results of Li's [33] research. At the same time, we also noticed that d_L is not completely consistent with d_R, which should be caused by manual errors in the fabrication process. It can also figure out that the total displacement of ACDEA is the sum of d_L and d_R, that is, d_t. For a common single cone actuator, the displacement is only d_L or d_R. Therefore, a significant increase in displacement would be beneficial in improving pump performance. The dotted lines in Fig. 8(b) indicate the theoretical results. As the voltage increases, the displacement gradually increases, and the changing trend of the curve is consistent with the experimental results.

As shown in Fig. 9, similar to the case where the displacement changes with voltage, the blocked force gradually increases as the voltage increases and the blocked force of the left and right parts of the ACDEA are also not completely the same, but it can be shown that the larger pre-stretching significantly increases the blocked force. The theoretical results of the blocked force are also consistent with the experimental results, but the values are slightly higher. The reason for this phenomenon may be that the material parameters used are not very accurate. In the theoretical calculation, the voltage applied to the membrane ranges from the inner to the outer boundary. However, the inner diameter of the ring-shaped electrode in the experiment is set to be larger than the outer diameter of the cylindrical block to prevent premature electric field breakdown and better use of the outer region of the membrane. For this kind of pump, a higher blocked force means higher pump pressure. Hence a higher pre-stretch within a certain range can be used to improve the pressure of the

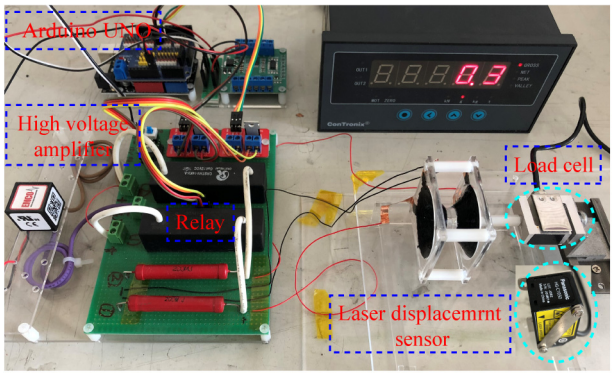

Fig. 7. Controlling and measuring system for experimental setup.

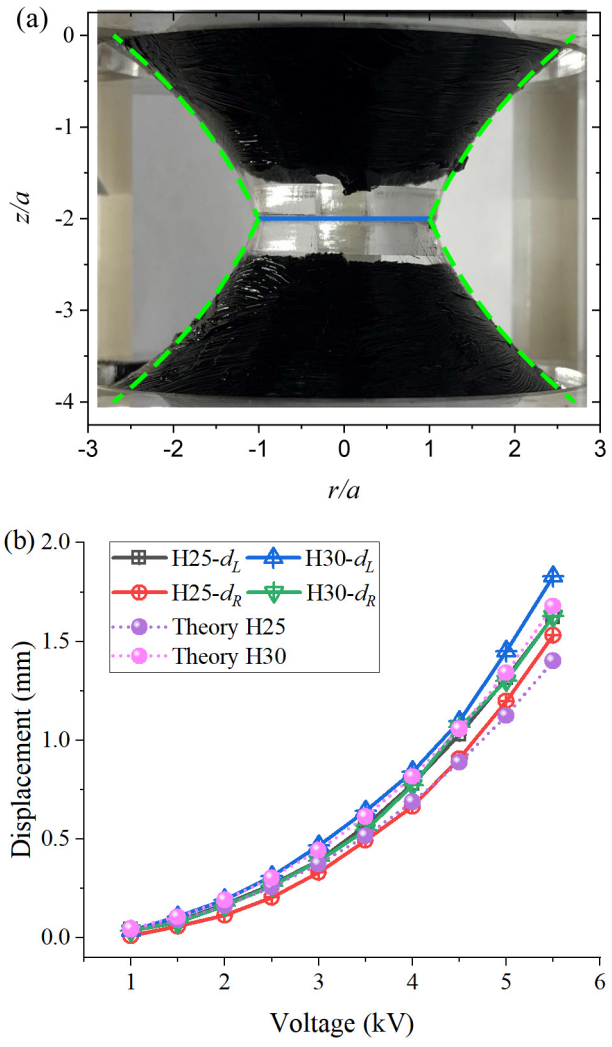

Fig. 8. Theoretical and experimental results of (a) the cross section of the antagonistic cone dielectric elastomer actuator in the reference state and (b) variation of displacement with voltage. . (For interpretation of the references to color in this figure legend, the reader is referred to the web version of this article.)

pump. Following previous research [18], more layers of dielectric elastomer membrane also can be used to increase the pump pressure.

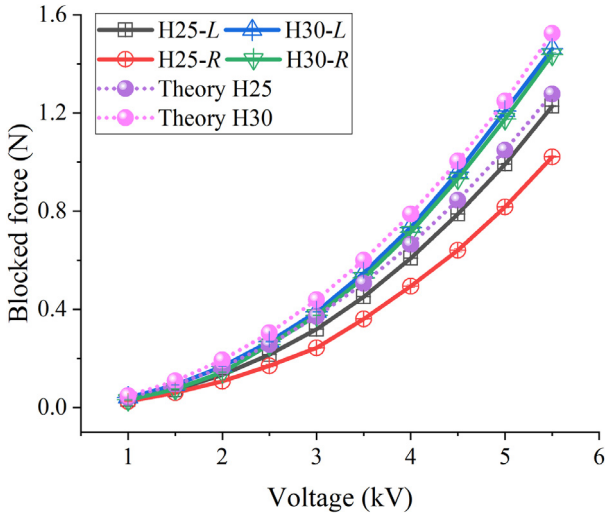

Fig. 9. Blocked force–voltage curves of the antagonistic cone dielectric elastomer actuator.

Next, we analyze the impact of voltage and frequency on the dynamic performance of the ACDEA. Fig. 10 depicts the displacement at different voltages and frequencies. As the voltage increases and the frequency decreases, the ACDEA can achieve greater displacement, seen in Fig. 10(a). The reason for this phenomenon is that the increase of the frequency makes the ACDEA voltage-on time decrease so that ACDEA cannot reach maximum displacement from the equilibrium position, as shown in Fig. 10(b). The viscoelasticity of VHB material also significantly affects the response speed of the actuator. When the frequency is further increased to a certain value, the system will resonate, causing ACDEA to obtain a greater displacement under strong vibration conditions. To capture the working conditions of the artificial heart, no consideration is given to the performance of ACDEA under resonance. Consistent with the static displacement test results, H30 has a better dynamic performance than H25.

4.2. ACDEP performance

Fig. 11 has revealed the ACDEP performance with the frequency and voltage variation. As previously considered that the larger displacement of the ACDEA can cause the pump to generate a greater average flow rate, but the trend of the curves in Fig. 11(a) is not the case. When the voltage is fixed, as the frequency increases, the average flow rate increases, peaks at 1.75 Hz, and then gradually decreases. This phenomenon is caused by the viscoelasticity of the VHB material. At the moment when the voltage is applied, the ACDEA deforms sharply. With the extension of time, the ACDEA has reached a larger displacement point. The ACDEA can go through multiple cycles during this time, and the cumulative displacement is more than a single cycle. So as the frequency increases, the average flow rate increases. If we consider the per-cycle pump volume, as shown in Fig. 11(b), a larger displacement can produce a larger volume of pumped water. When the cumulative displacement of the ACDEA in 1 s reaches the maximum value, that is, the frequency is 1.75 Hz, the average flow rate also reaches the maximum value. As the frequency increases further, the ACDEA cannot reach a larger displacement from the equilibrium position, and the cumulative displacement becomes smaller resulting in the average flow rate gradually decreasing. Compared with H25, H30 has a higher average flow rate, with a maximum of 134.27 mL/min and per-cycle pump volume, with a maximum of 2.27 mL.

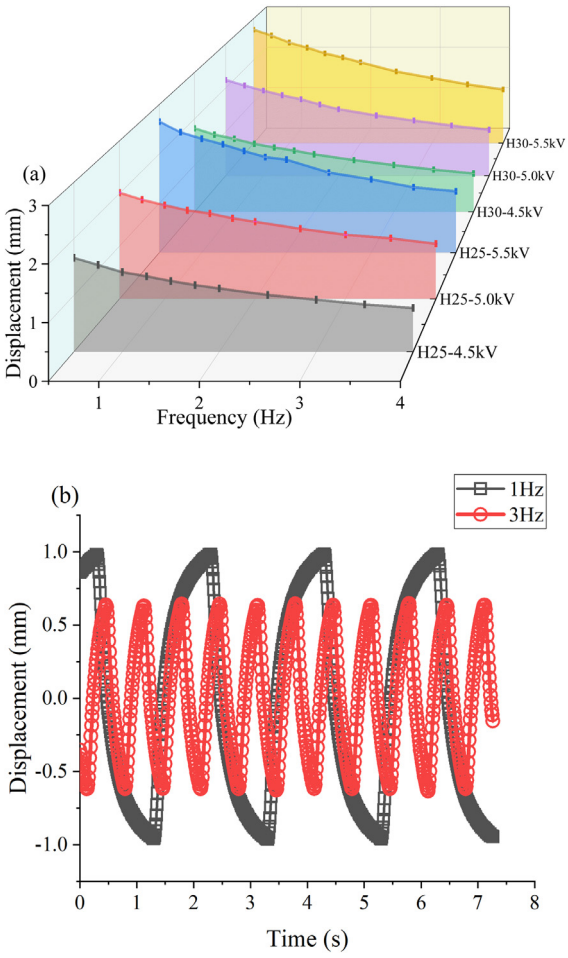

Fig. 10. The dynamic performance of the antagonistic cone dielectric elastomer actuator. (a) Displacement at different voltages and frequencies. (b) Displacement–time curves at different frequencies.

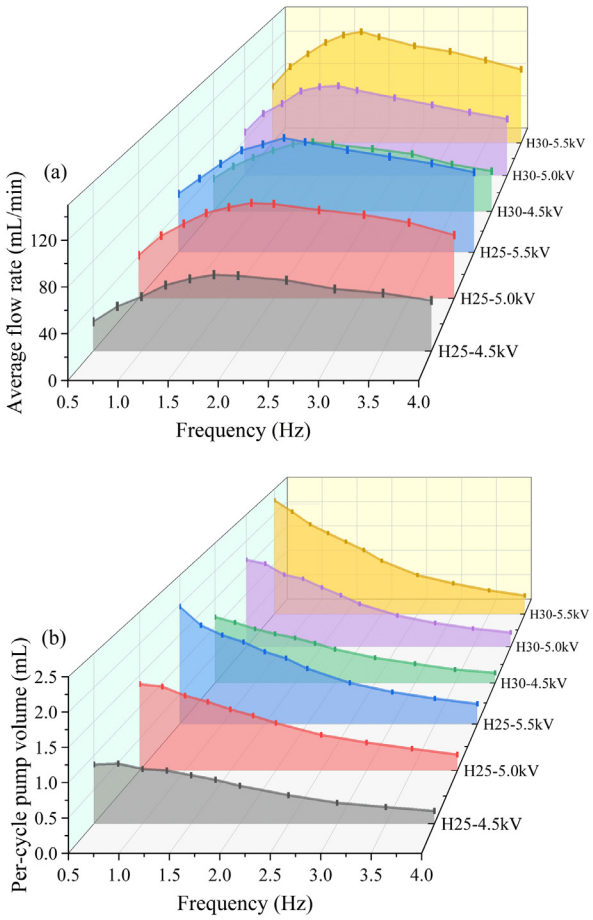

Fig. 11. The flow rate of the pump. (a) Average flow rate at different voltages and frequencies. (b) Per-cycle pump volume at different voltages and frequencies.

Fig. 12 shows the maximum pump pressure at different voltages and frequencies. As the voltage increases and the frequency decreases, the pump can achieve higher pump pressure. When the frequency of the pump is low, the pump pressure is mainly maintained by the blocked force and closed check valve. As the frequency increases, the uninterrupted opening and closing of the check valve causes the pump pressure to be unsustainable, so the pump pressure decreases. The maximum pump pressure of H30 is 15.78 mbar, which is greater than that of H25. As we have considered before, a larger blocked force can generate a higher pump pressure.

To compare the performance of ACDEP with other pumps based on dielectric elastomer, the most important parameters are summarized in Table 1. It is shown that this work can provide a larger flow rate at low frequencies. Although the flow rate is lower than the peristaltic pump [34], the size of the ACDEP is much smaller, and the driving voltage is also lower.

The presented pump has good performance at low frequencies, and there is almost no noise and vibration. The working principle of the pump is similar to the human heart, and the working frequency of its best performance falls within the range of the human heart. It has great potential as an artificial heart. PDMS membrane can be used to replace VHB material, and conductive gel can be used as compliant electrodes to improve the biological affinity of the pump. We also realize that there are still many challenges in the actual application of the pump, such as lower average flow rate and pressure. The voltage used to actuate the pump also needs to be reduced. In addition, the performance of the pump can be improved through a variety of methods. For example, when the size of the pump is larger, the average flow rate and per-cycle pump volume of the pump can be improved, and more layers of dielectric elastomer membrane can also be used to increase the pressure. With a better performance, the pump will also be used in more applications, such as replacing traditional peristaltic pump in experiments.

5. Conclusion

In summary, a theoretical model for the antagonistic cone dielectric elastomer actuator was derived, and the theoretical results have better tally with experimental results. Higher displacement and blocked force can be obtained by adjusting the height of the ACDEA to allow the dielectric membrane to achieve a larger pre-stretch. Inspired by the human heart, a pump was developed and its performance was investigated experimentally. Due to the viscoelasticity of the material, the pump can obtain a maximum pump volume per cycle at a very low frequency. The pump reaches the maximum average flow rate of 134.27 mL/min at 1.75 Hz and there was almost no noise and vibration during operation. It is promising as an artificial heart.

In this study, we have only developed statics theoretical model and conducted experimental verification. Although the theoretical results agree well with the experimental results, which can

Table 1
Performance comparison of pumps based on dielectric elastomer with different designs.

Type	Average flow rate (mL/min)	Pressure (kPa)	Frequency (Hz)	Voltage (kV)	Size (d: diameter; l: length; h: height) (mm)
All-polymer micropumps [35]	0.077	8.45	5–150(30)	3.3	less than 10 mm^2 of chip space
Microfluidic pump with bucking of DE plates [36]	1.2	0.5	0.07	5.5–7.5	13.5(d)
Peristaltic pump module [37]	/	0.51	2	0–10	45(d) × 80(l)
Micropump with a pull-up spring [13]	2.52	/	0.1–8(3)	0–4.2	100(d)
Peristaltic pump [34]	2.5 × 10^3	0–4	0–7(1.5)	0–10	45(d) × 90(l) (single pump module)
Presented work	134.27	1.578	0.5–4(1.75)	4.5–5.5	40(d) × 30(h)

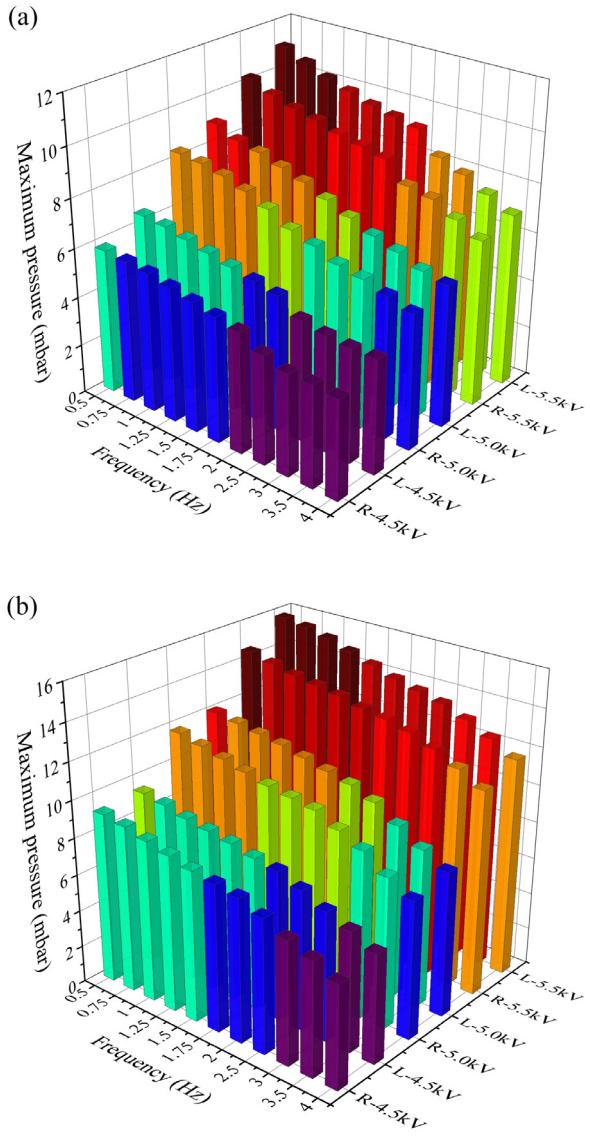

Fig. 12. Pump pressure of (a) H25 and (b) H30 at different voltages and frequencies.

guide the design and explain electromechanical behavior of the ACDEA, there are still many deficiencies. The viscoelasticity of the material will significantly affect the performance of the ACDEA. This kind of actuator often works under a dynamic condition, such as a pump, and a dynamic model is required to guide the design and application of the actuator. It is hoped that this work can guide the development of the ACDEA and inspire the novel design of the dielectric elastomer actuator that can be applied in various environments.

Declaration of competing interest

The authors declare that they have no known competing financial interests or personal relationships that could have appeared to influence the work reported in this paper.

Acknowledgment

This work is supported by the National Natural Science Foundation of China (Grant No. 11772109).

Appendix A. Supplementary data

Supplementary material related to this article can be found online at https://doi.org/10.1016/j.eml.2020.101134.

References

[1] J. Li, L. Liu, Y. Liu, J. Leng, Dielectric elastomer spring-roll bending actuators: Applications in soft robotics and design, Soft Robot. 6 (2019) 69–81.
[2] J. Shintake, B. Schubert, S. Rosset, H. Shea, D. Floreano, Variable stiffness actuator for soft robotics using dielectric elastomer and low-melting-point alloy, in: 2015 Ieee/Rsj International Conference on Intelligent Robots and Systems (Iros), 2015, pp. 1097–1102.
[3] G. Kofod, M. Paajanen, S. Bauer, Self-organized minimum-energy structures for dielectric elastomer actuators, Appl. Phys. A 85 (2006) 141–143.
[4] R. Baumgartner, A. Kogler, J.M. Stadlbauer, C.C. Foo, R. Kaltseis, M. Baumgartner, G. Mao, C. Keplinger, S.J.A. Koh, N. Arnold, Z. Suo, M. Kaltenbrunner, S. Bauer, A lesson from plants: High-speed soft robotic actuators, Adv. Sci. 7 (2020) 1903391.
[5] X.F. Lv, L.W. Liu, Y.J. Liu, J.S. Leng, Dielectric elastomer energy harvesting: maximal converted energy, viscoelastic dissipation and a wave power generator, Smart Mater. Struct. 24 (2015) 115036.
[6] J. Zhou, L. Jiang, R. Khayat, Analysis on the energy harvesting cycle of dielectric elastomer generators for performance improvement, Europhys. Lett. 115 (2016) 27003.
[7] B. Huang, M. Li, T. Mei, D. McCoul, S. Qin, Z. Zhao, J. Zhao, Wearable stretch sensors for motion measurement of the wrist joint based on dielectric elastomers, Sensors (Basel) 17 (2017) 2708.
[8] J. Liu, G. Mao, X. Huang, Z. Zou, S. Qu, Enhanced compressive sensing of dielectric elastomer sensor using a novel structure, J. Appl. Mech. 82 (2015) 101004.
[9] J.R. Li, Y. Wang, L.W. Liu, S. Xu, Y.J. Liu, J.S. Leng, S.Q. Cai, A biomimetic soft lens controlled by electrooculographic signal, Adv. Funct. Mater. 29 (2019) 1903762.
[10] C. Christianson, N.N. Goldberg, D.D. Deheyn, S. Cai, M.T. Tolley, Translucent soft robots driven by frameless fluid electrode dielectric elastomer actuatorsl, Sci. Robot. 17 (2018) eaat1893.
[11] T. Li, G. Li, Y. Liang, T. Cheng, J. Dai, X. Yang, B. Liu, Z. Zeng, Z. Huang, Y. Luo, T. Xie, W. Yang, Fast-moving soft electronic fish, Sci. Adv. 3 (2017) e1602045.
[12] T. Li, Z. Zou, G. Mao, X. Yang, Y. Liang, C. Li, S. Qu, Z. Suo, W. Yang, Agile and resilient insect-scale robot, Soft Robot. 6 (2018) 133–141.
[13] F.A. Mohd Ghazali, C.K. Mah, A. AbuZaiter, P.S. Chee, M.S. Mohamed Ali, Soft dielectric elastomer actuator micropump, Sensors Actuators A 263 (2017) 276–284.
[14] T. Yang, Y. Xiao, Z. Zhang, Y. Liang, G. Li, M. Zhang, S. Li, T.W. Wong, Y. Wang, T. Li, Z. Huang, A soft artificial muscle driven robot with reinforcement learning, Sci. Rep. 8 (2018) 14518.
[15] S. Hau, G. Rizzello, M. Hodgins, A. York, S. Seelecke, Design and control of a high-speed positioning system based on dielectric elastomer membrane actuators, IEEE/ASME Trans. Mechatronics 22 (2017) 1259–1267.

[16] M. Hodgins, A. York, S. Seelecke, Experimental comparison of bias elements for out-of-plane DEAP actuator system, Smart Mater. Struct. 22 (2013) 094016.
[17] H.-m. Wang, J.-y. Zhu, K.-b. Ye, Simulation, experimental evaluation and performance improvement of a cone dielectric elastomer actuator, J. Zhejiang Univ.-Sci. A 10 (2009) 1296–1304.
[18] S. Hau, G. Rizzello, S. Seelecke, A novel dielectric elastomer membrane actuator concept for high-force applications, Extreme Mech. Lett. 23 (2018) 24–28.
[19] M. Follador, M. Cianchetti, B. Mazzolai, Design of a compact bistable mechanism based on dielectric elastomer actuators, Meccanica 50 (2015) 2741–2749.
[20] M. Hodgins, A. York, S. Seelecke, Modeling and experimental validation of a bi-stable out-of-plane DEAP actuator system, Smart Mater. Struct. 20 (2011) 094012.
[21] C.T. Nguyen, H. Phung, H. Jung, U. Kim, T.D. Nguyen, J. Park, H. Moon, J.C. Koo, H.R. Choi, Printable monolithic hexapod robot driven by soft actuator, in: 2015 Ieee International Conference on Robotics and Automation (Icra), 2015, pp. 4484–4489.
[22] C.T. Nguyen, H. Phung, P.T. Hoang, T.D. Nguyen, H. Jung, H. Moon, J.C. Koo, H.R. Choi, A novel bioinspired hexapod robot developed by soft dielectric elastomer actuators, in: 2017 Ieee/Rsj International Conference on Intelligent Robots and Systems (Iros), 2017, pp. 6233–6238.
[23] G. Rizzello, M. Hodgins, D. Naso, A. York, S. Seelecke, Modeling of the effects of the electrical dynamics on the electromechanical response of a DEAP circular actuator with a mass–spring load, Smart Mater. Struct. 24 (2015) 094003.
[24] S. Hau, A. York, G. Rizzello, S. Seelecke, Performance prediction and scaling laws of circular dielectric elastomer membrane actuators, J. Mech. Des. 140 (2018) 113501.
[25] T. He, X. Zhao, Z. Suo, Dielectric elastomer membranes undergoing inhomogeneous deformation, J. Appl. Phys. 106 (2009) 083522.
[26] G. Mao, L. Wu, Y. Fu, J. Liu, S. Qu, Voltage-controlled radial wrinkles of a trumpet-like dielectric elastomer structure, AIP Adv. 8 (2018) 035314.
[27] L. Meng, F. Li, H. Li, Dynamic model and analysis of a dielectric elastomer vibration isolator, J. Intell. Mater. Syst. Struct. 30 (2019) 2396–2404.
[28] A.N. Gent, A new constitutive relation for rubber, Rubber Chem. Technol. 69 (1996) 59–61.
[29] A three-dimensional constitutive model for the large stretch behavior of rubber elastic materials, 41 (1993) 389–412.
[30] M. Mooney, A theory of large elastic deformation, J. Appl. Phys. 11 (1940) 582–592.
[31] T.-Q. Lu, Z.-G. Suo, Large conversion of energy in dielectric elastomers by electromechanical phase transition, Acta Mech. Sinica 28 (2012) 1106–1114.
[32] F. Wang, C. Yuan, T. Lu, T.J. Wang, Anomalous bulging behaviors of a dielectric elastomer balloon under internal pressure and electric actuation, J. Mech. Phys. Solids 102 (2017) 1–16.
[33] B. Li, H. Chen, J. Qiang, S. Hu, Z. Zhu, Y. Wang, Effect of mechanical pre-stretch on the stabilization of dielectric elastomer actuation, J. Phys. D: Appl. Phys. 44 (2011) 155301.
[34] G. Mao, L. Wu, Y. Fu, Z. Chen, S. Natani, Z. Gou, X. Ruan, S. Qu, Design and characterization of a soft dielectric elastomer peristaltic pump driven by electromechanical load, IEEE/ASME Trans. Mechatronics 23 (2018) 2132–2143.
[35] J.J. Loverich, I. Kanno, H. Kotera, Concepts for a new class of all-polymer micropumps, Lab Chip 6 (2006) 1147–1154.
[36] B. Tavakol, M. Bozlar, C. Punckt, G. Froehlicher, H.A. Stone, I.A. Aksay, D.P. Holmes, Buckling of dielectric elastomeric plates for soft, electrically active microfluidic pumps, Soft Matter 10 (2014) 4789–4794.
[37] G. Mao, X. Huang, J. Liu, T. Li, S. Qu, W. Yang, Dielectric elastomer peristaltic pump module with finite deformation, Smart Mater. Struct. 24 (2015) 075026.